NEXT Single String Integration Tests in Support of the Double Asteroid Redirection Test Mission

IEPC-2019-853

Presented at the 36th International Electric Propulsion Conference
University of Vienna • Vienna, Austria
September 15-20, 2019

Robert E. Thomas[1] and Michael V. Aulisio[2]
NASA Glenn Research Center, Cleveland, OH, 44135, USA

Andrew R. Badger[3], Christopher C. Heistand[4], Derik S. Thompson[5], Raymond Liang[6], and Jeremy John[7]
Johns Hopkins University Applied Physics Laboratory, Laurel, MD, 20723, USA

Keith D. Goodfellow[8]
Aerojet Rocketdyne., Redmond, WA, 98073, USA

and

James J. Bontempo[9]
Zin Technologies Inc., Cleveland, OH, 44139, USA

Abstract: A system integration test has been performed utilizing a prototype model NEXT ion thruster, an engineering model power processing unit, and a laboratory model command and data handling system. The objectives of the test were to: a) verify that the integrated system meets performance requirements, b) demonstrate that the integrated system is functional across the anticipated thermal, power processor, and Xe propellant ranges for the DART mission, and to c) evaluate fault detection and operation of the command and data handling system. Measurements made during this test included: thruster performance, PPU input voltages, PPU electrical and thermal telemetry, software states, and fault flags. Additionally, a far-field electrostatic probe diagnostic was used to infer relative changes in the thrust vector across the various propellant flow splits. This manuscript presents the results of these tests, which include integrated ion propulsion system demonstrations of performance, details on the execution of DART flight algorithms, and software fault handling.

[1] Aerospace Engineer, Electric Propulsion Systems Branch, robert.e.thomas@nasa.gov.
[2] Electrical Engineer, Power Management and Distribution Branch, michael.v.aulisio@nasa.gov.
[3] Flight Software Developer, Intelligent Systems Group, Andrew.Badger@jhuapl.edu.
[3] DART Flight Software Lead, Embedded Software Group, Christopher.Heistand@jhuapl.edu.
[5] Testbed Developer, Acoustic Systems Group, Derik.Thompson@jhuapl.edu.
[6] Contamination Modeling Scientist, Space Hardware Procurement, Material Science, and Environmental Effects Group, Ray.Liang@jhuapl.edu.
[7] DART Propulsion Lead, Mechanical Systems Group, Jeremy.John@jhuapl.edu.
[8] Chief Engineer, Arcjet Thruster Systems, Keith.Goodfellow@Rocket.com.
[9] Electrical Engineer, ZIN Technologies, bontempoj@ZIN-TECH.COM

Nomenclature

J_a = accelerator current, A
J_b = beam current, A
J_d = discharge current, A
V_g = coupling voltage, V
V_d = discharge voltage, V

I.Introduction

NASA's Double Asteroid Redirection Test (DART) will be the first-ever mission to demonstrate asteroid deflection using kinetic impactor technology. The target for the DART mission is the binary asteroid system Didymos, which is composed of two asteroids: a 780 m diameter asteroid Didymos A, and its 160 m diameter moonlet Didymos B. The DART spacecraft will impact Didymos B and earth-based telescopes will measure its corresponding change in orbit. The DART mission recently passed its Mission Critical Design Review, and is led by Johns Hopkins University Applied Physics Laboratory (APL). The DART spacecraft will utilize the NASA Evolutionary Xenon Thruster (NEXT), which is a successor to the NSTAR ion propulsion system that successfully propelled NASA's Deep Space 1 and Dawn spacecraft. By utilizing electric propulsion, DART is able reduce the amount of propellant required for trajectory control maneuvers and gain flexibility in mission operations.

The NEXT ion propulsion system was developed at the NASA Glenn Research Center as part of a comprehensive technology development program.[1-7] In 2015 NASA contracted with Aerojet Rocketdyne and subcontractor Zin Technologies to manufacture two thrusters and two power processing units (PPUs) for use on future NASA missions. This ongoing effort is called the NEXT-Commercial (NEXT-C) project.[8,9] The objectives of the NEXT-C program are to reduce the cost of the propulsion system to potential mission users, mature the design to TRL 8, and produce two flight thrusters and two flight power processing units to be provided as government furnished equipment to the first mission users. The first NEXT-C propulsion string will be delivered to APL for use on DART, while the second string is being reserved as a backup for the mission.

A single string integration test (SIT) has been performed on the NEXT propulsion system as part of the DART system validation process. The tests incorporated a prototype model thruster, an engineering model PPU, and a laboratory model command and data handling system. The objectives of this test were to verify that the integrated system meets performance requirements, demonstrate that the integrated system is functional across the anticipated power processor and propellant input ranges, and to evaluate fault detection and operation of the command and data handling system. The results of this test were used in the development of the flight software, which will be tested with flight hardware (thruster + PPU) in the fall of 2019. This manuscript will present test results of the integration test. The next section details the software and hardware used to conduct the test. The test plan is then detailed, followed by the test results and the summary.

II.Propulsion System Element Descriptions

This section details the hardware and software used in the integration test. This includes descriptions of the ion thruster, power processing unit, and the software in the loop simulator (SWIL).

A. Ion Thruster

The 'Dev-C' prototype-model thruster was used during the integration test. The Dev-C thruster is a re-worked version of the PM1R thruster, which has been extensively documented and tested.[10-13] As noted in Ref. 8, Aerojet Rocketdyne made several changes to the thruster design as part of the NEXT-C project:

- The configuration of the propellant connections were modified to aid in the manufacturing process;
- Propellant connections were changed to tube stubs to better facilitate integration to the spacecraft;
- Harness materials were changed to increase thermal margins;
- The mounting hardware was modified to meet strength and stiffness requirements.

These changes were made to improve the manufacturability of the engine, while not invalidating the performance or lifetime capabilities of the original design. The Dev-C thruster underwent performance tests after these changes were made to the engine, which included random vibration and shock tests. It was found that the changes did not appreciably affect the functional performance of the engine. A photograph of the Dev-C thruster mounted in test facility is shown in Fig. 1.

Figure 1. Dev-C engine mounted in VF-16 prior to pump down.

B. Power Processing Unit

The PPU used during testing was an engineering model unit that was built by Zin Technologies, which has significant heritage to the unit that was developed by L3 Technologies during the NEXT Phase II development program.[14,15] Figure 2 shows a block diagram of the six power supplies used to power the thruster. The supplies process power over a wide range of input voltages and output power levels, and a "slice" circuit transmits controls, status, and telemetry through a RS-485 interface to the SWIL simulator. The beam supply processes approximately 85% of the total power at DART conditions and consists of six addressable power modules that operate in parallel. The discharge supply provides power for ionization and processes approximately 10% of the power. The remaining 5% is processed by the accelerator, neutralizer keeper, neutralizer heater, and discharge heater supplies; these four power supplies share common primary side switching transistors and are referred to as the quad supply. A module addressing circuit, controlled by the SWIL simulator, selects the number of operational beam modules. Unused modules can be turned off to increase efficiency because housekeeping power consumption is reduced while the remaining modules are operated closer to optimum load conditions.

A 22-34 VDC low power bus is used by the PPU for housekeeping functions and an unregulated 80-160 VDC high power bus powers the six supplies. High and low power bus power to the PPU was provided by voltage regulated, commercially available power supplies. The PPU also has internal fault protection to shut-down from a high power bus under- or overvoltage, or from a low power bus under-voltage. The PPU also provides recycle control and fault protection from neutralizer and discharge extinctions, and for recycle rates exceeding a predefined recycle level.

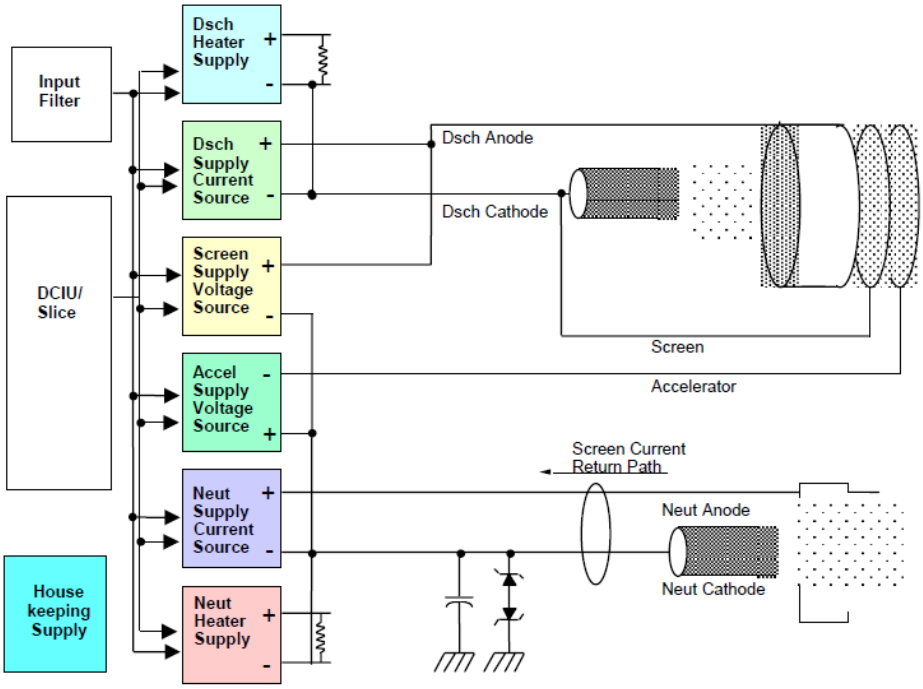

Figure 2. Schematic of the NEXT PPU (the beam supply is labeled as the "screen" supply).

C. Software-In-The-Loop Environment

DART's development environment revolves around the enhanced SWIL environment which enables flight software development and testing of Flight Software on commercial off-the-shelf (COTS) machines. The SWIL provides an early, medium-fidelity test environment that can easily scale for extensive test regimes by allowing a developer to practically have a spacecraft on a laptop. The DART team achieves this concept by including the Flight Software (FSW), Testbed Software (TBSW), and Ball Aerospace COSMOS ground software (GSW) in a single machine with no need for specialized hardware.

This environmental segmentation is achieved via Docker, allowing each application to run standalone with a controlled and independent system configuration. FSW, TBSW, and COSMOS each have individual, stateless containers that Docker Compose builds and orchestrates. Docker Compose creates the network of services in containers with mounted volumes from the local machine. The resulting system is a complete SWIL testbed environment that is consistent for both software development and automated testing.

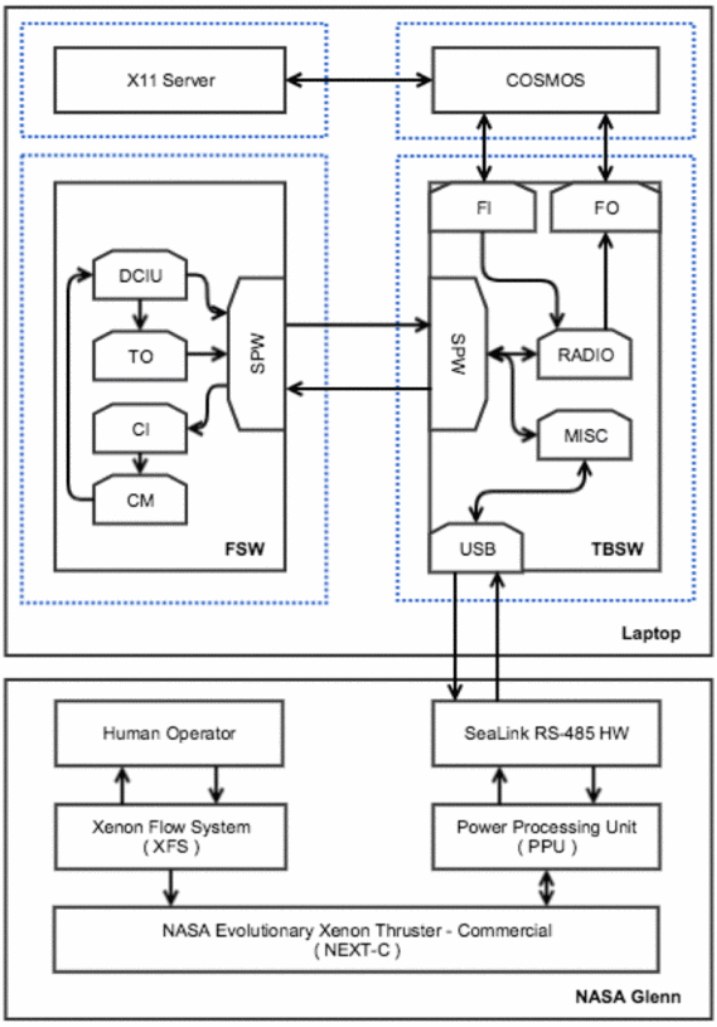

Figure 3. SWIL block diagram.

The SWIL's ability to exercise real Flight Software code with emulated flight hardware, ground system, and NEXT-C allows DART to approach an emulated test-as-you-fly style system even without avionics hardware. The DART FSW is built on Goddard's core Flight Executive (cFE), providing an additional layer of hardware abstraction between flight hardware and pc-linux. APL built applications such as digital control interface unit (DCIU), continuous integration (CI), and configuration management (CM) provide a commanding and telemetry path from ground to spacecraft to the NEXT-C ion thruster through the PPU.[16]

Communication with the PPU required the interlacing of the four Docker containers that make up SWIL, the host Linux PC, and the use of commercial of the shelf hardware as shown in Fig. 3. Utilizing COSMOS, PPU commands are sent to FSW, through the avionics emulation in test-bed to the PPU. The avionics emulation includes a PPU Interface application, used to connect the host PC USB drivers to the PPU via the Sealink USB to 2-Port RS-485 box. The system was modified from the original NEXT-C interface control document (ICD) that required two-way communication across both ports to transmitting five byte commands over port-1 and receiving five byte replies over port-2. This stream lined communication where redundancy was not required.

D. Xenon Feed System

Commercial mass flow controllers were used to provide high-purity Xe to the thruster. The xenon flow system (XFS) was located on the atmospheric side of vacuum facility 16 (VF-16) and provided independent flow control to each of the three thruster propellant inputs: neutralizer, cathode, and main. Tubing and components of the XFS were wrapped with heater tape during a bake-out procedure to remove air and adsorbed moisture on surfaces exposed to atmosphere. The flows were controlled manually during the tests. The telemetry from the mass flow controllers were recorded using a data acquisition system.

III. Test Apparatus

The system integration test was conducted in two independently controlled vacuum facilities. The test setup and vacuum facilities are described in this section.

A. Test Facilities

The thruster was operated in VF-16 at NASA GRC. The cryogenically pumped facility is 2.7 meters in diameter and 8.5 meters in length, with a base pressure of 2.7×10^{-5} Pa (2.0×10^{-7} torr). The facility pressure, corrected for

xenon, during TL28 operation was 3.1 x 10^{-4} Pa (2.3 x 10^{-6} torr). The facility's interior surfaces were lined with graphite to reduce the amount of back-sputtered material onto the thruster. A data acquisition was used to monitor the facility pressure and mass flow rates. Data were sampled at a frequency of 10-20 Hz, and written to a file at rate of 1 Hz during thruster operation.

The PPU was operated in a dedicated facility to protect it from back-sputtered facility material and to allow for quicker problem resolution should the unit require atmospheric exposure for servicing. The PPU was mounted within NASA GRC's Vacuum Facility 14 (VF-14), which is shown in Fig. 4 The dimensions of the facility are 0.56 m x 0.56 m x 0.91 m and it was evacuated with a turbo-molecular pump. Facility pressures were typically 2.7×10^{-4} Pa (2×10^{-6} Torr) during PPU operation. The PPU was mounted on a cold plate for removal of PPU waste heat. The cold plate was an aluminum alloy plate with machined internal passages for the cooling fluid. A high thermal conductivity gasket was used as an interface material to ensure a good thermal contact between the PPU thermal interface and cold plate.

The prototype PPU was instrumented with internal and external thermocouples for monitoring component temperatures, design assessment, and thermal analysis validation. A heat exchanger controlled the PPU reference thermocouple to a predefined value throughout all tests. All of the thermocouples were monitored by a separate data logging computer. The PPU was tested with both the thruster and on a resistive load for requirements verification and validation. The PPU outputs were wired through a breakout box (BoB) that allowed for independent measurements of PPU output currents and voltages. Oscilloscopes were used to measure current and voltage transients during recycles and cathode ignition. The SWIL simulator also monitored and recorded all digital telemetry from the PPU. This telemetry included all PPU power supply output voltages and currents, as well as the high and low power bus input voltages and currents. All measured voltages that were used to verify and validate PPU operation were measured as close as possible to the PPU to eliminate voltage drops. Oscilloscope traces were stored electronically.

Figure 4. PPU mounted within VF-14.

A schematic and photograph of the apparatus are shown in Figs. 5 and 6, respectively.

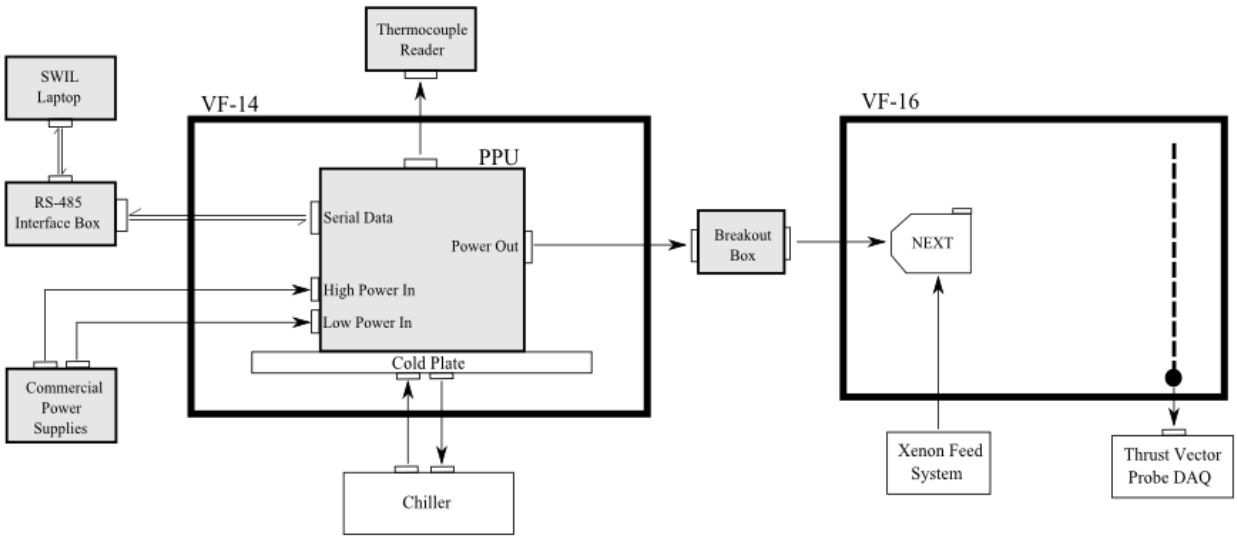

Figure 5. Block diagram of the integration test facilities.

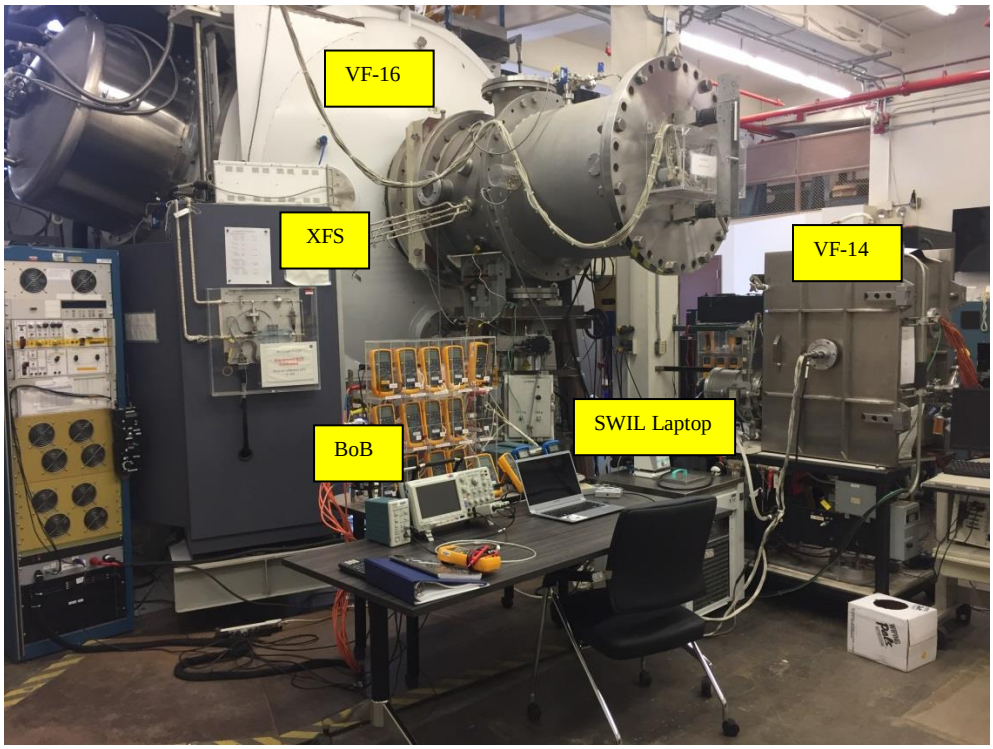

Figure 6. Physical layout of the system integration test facilities.

B. Thrust Vector Diagnostic

An 18 x 18 array of graphite rods were used to measure the far-field beam current centroid, which was used to infer relative changes in the thrust vector. Each graphite rod has a diameter of 0.19 cm and a length of 152 cm, and had an identical surface finish and small radial tolerance (1 mil). The probes were mounted within a graphite covered stainless steel frame approximately 719 cm downstream from the exit plane of the thruster. The rods were biased 30 V below ground and the rod currents were measured across a shunt bank. The system was calibrated by passing known currents through the rods and measuring the response on the data acquisition computer. A laser alignment tool was used to align the thruster with the center of the probe array. The probes were mounted in VF-16 as shown in Fig. 7.

Figure 7. Far-field probe assembly used for characterizing the thrust vector.

C. Data Regression Test

As a precursor to the SIT, DART's SWIL environment was exercised on test-beds of increasing fidelity using a uniform test suite designed to evaluate the state-based logic of DART's implementation of NEXT-C's operating sequences. Each algorithm is encoded in a single configuration file as a series of state transitions within the Flight Software (FSW) controller. The Digital Control Interface Unit (DCIU) core flight executive (cFE) Flight Software application is responsible for commanding the PPU and managing sequence execution via finite state machines (FSM), while polling the PPU for NEXT-C telemetry. Each NEXT-C telemetry point is identified by a PPU command code, and each state of the operating sequences is captured with a unique identifier (UID) within FSW. The sequence configuration contains rows for each FSW FSM state UID and columns for each PPU command code along with meta data for timing; this configuration captures the expected reported state of NEXT-C at each point of sequence execution.

DART's SWIL simulator contains a test pipeline that commands the NEXT-C thruster to run a given sequence, and record DCIU/PPU telemetry during its execution. Each second, the telemetered FSM state UID is compared against the expected UID according to the sequence configuration file. If the telemetered FSM state UID does not succeed the correct state UID according to the sequence configuration, an error is thrown. If any of the NEXT-C telemetry values defined for this FSM state is invalid or out of range, an error is thrown. This test apparatus enabled DART to synchronize the definition of each NEXT-C sequence with its software implementation.

Prior to the SIT, DART leveraged this test infrastructure to test its DCIU NEXT-C controller with:

- A SWIL system with a basic software emulation of PPU messaging
- A physical PPU command and telemetry (PCAT) connected to a SWIL laptop

The initial software test configuration connected DART's FSW to an endpoint that could receive and send PPU commands/telemetry; this first test did not have any state/logic for the ion engine, but enabled DART to validate its messaging formats. The addition of the NASA's higher fidelity PCAT PPU emulation allowed DART to test the NEXT-C sequences in software prior to the SIT.

During SIT, DART exercised this test platform to evaluate the DCIU NEXT-C controller with:

- DCIU communicating with NEXT-C's PPU running against a load bank
- DCIU communicating with NEXT-C's PPU running the NEXT-C thruster

IV.Test Plan

The system integration test plan included propulsion system demonstrations of performance, functionality, and fault handling. Propulsion system demonstrations of performance included measurements at standard input conditions over the range of anticipated propellant flow and PPU input conditions. The PPU was operated at a baseplate at the maximum acceptable flight temperature of 55 °C to verify systems interfaces at elevated temperatures. Table 1 lists the various PPU and flow input parameters that were tested.

Table 1. System Integration Test Parameters

Test Parameter	Range
PPU Baseplate Temperatures	-24 °C, 40 °C, 55 °C
Propellant Flow Rates	Main: +7% and -5% of nominal flow value Disch. Cathode: +/- 6% of nominal flow value Neut. Cathode: +21% and -6% of nominal flow value
PPU High Power Bus Input Voltages	80 V, 100 V, 125 V
PPU Low Power Bus Input Voltage	28 V
Throttle Levels	DETL2.7A, DTL28, DTL29

Measurements made during these tests included: thruster currents and voltages as measured from the PPU breakout-box, PPU input voltages, Xe flows to the thruster, PPU electrical and thermal telemetry recorded by SWIL, SWIL states, and fault flags. Additional measurements included: ripples on PPU regulated and unregulated parameters; recycle behavior and accelerator grid surge current during start-ups; heater currents and voltages and ignitor waveforms during cathode ignitions; power bus transients during ignition, and monitoring PPU performance while the high power bus was ramped between 80 and 125 V. Demonstrations of fault handling were also conducted on a resistive load, in which PPU-related faults were simulated and the system response to these faults was monitored by the SWIL simulator. Demonstrations of system safing due to a high recycle rate, a PPU high power bus voltage interlock on discharge and neutralizer low current, and power-on reset states of the SWIL simulator and PPU were also completed.

Prior to connecting the PPU to the thruster, the PPU was verified to be operating nominally under command by the SWIL simulator when its output was connected to a resistive load-bank. The PPU passed its functional testing with the resistive load-bank, which was a prerequisite for connecting it to the thruster. These functional tests included rehearsal of all sequences with the relevant settings for the three DART throttle levels.

NEXT engine performance was documented over the range of anticipated DART flight conditions. Testing was confined to the beam voltage and beam current envelope highlighted in Fig. 8. The DART mission will be performed exclusively at a beam current of 2.70A, with a baseline beam voltage of 1021 V. The adjacent throttle levels may be used depending on the available input power to the propulsion system. During the NEXT Phase II development program, all ground tests were conducted using xenon feed systems with a maximum flow tolerance of +/-3%. Given that NEXT will nominally operate at a single operating point during the DART mission, APL opted to use commercial-off-the-shelf flow restrictors to provide propellant to the engine. While this provides simplifications the xenon feed system, it came at the expense of a) reduced flow accuracy; and b) the inability to throttle flows, which is typically done during NEXT startup operations. Risk reduction tests (RRT) were conducted at The Aerospace Corporation, focusing on characterizing engine performance and erosion characteristics within the tolerance bands of the chosen flow restrictors.[17] The results on the system integration tests were compared to the baseline RRT data.

In the following sections, the DTLXX-Y-Z flow rate nomenclature designates a DART throttle condition. The D denotes that the throttle level is DART-specific, Y indicates the total discharge chamber flow rate (main + cath) and Z designates the neutralizer flow rate. The discharge flow splits that were investigated during testing are shown in Fig. 9. The highest flow rate is designated with an “A”, “O” is the lowest, and “H” is the nominal flow. The nominal condition for the DART mission is DTL28-H-H. The flow restrictors nominally have a flow tolerance of +/- 3% on the main and +/- 6% on both cathodes. These conditions were tested during the initial phase of the integration test. As a follow-on risk-reduction activity, the flow envelope was then widened to the flows shown in

Table1 above. The DART throttle table showing the set-point flows, currents, and voltages is located in the Appendix.

	V_{bps}, V												
I_b, A	1800	1567	1396	1179	1021	936	850	700	679	650	400	300	275
3.52	TL40	TL39	TL38	TL37	ETL3.52A	ETL3.52B	ETL3.52C	ETL3.52D					
3.10	TL36	TL35	TL34	TL33	ETL3.1A	ETL3.1B	ETL3.1C	ETL3.1D	ETL3.1E				
2.70	TL32	TL31	TL30	TL29	TL28	ETL2.7A	ETL2.7B	ETL2.7C	ETL2.7D	ETL2.7E			
2.35	TL27	TL26	TL25	TL24	TL23	ETL2.35A	ETL2.35B	ETL2.35C	ETL2.35D	ETL2.35E			
2.00	TL22	TL21	TL20	TL19	TL18	ETL2.0A	ETL2.0B	ETL2.0C	ETL2.0D	ETL2.0E			
1.60	TL17	TL16	TL15	TL14	TL13	ETL1.6A	ETL1.6B	ETL1.6C	ETL1.6D	ETL1.6E	ETL1.6F		
1.20	TL12	TL11	TL10	TL09	TL08	TL07	TL06		TL05	TL04	TL03	TL02	
1.00													TL01

Figure 8. NEXT Throttle Table 11.1, with the highlighted region showing anticipated DART conditions.

.

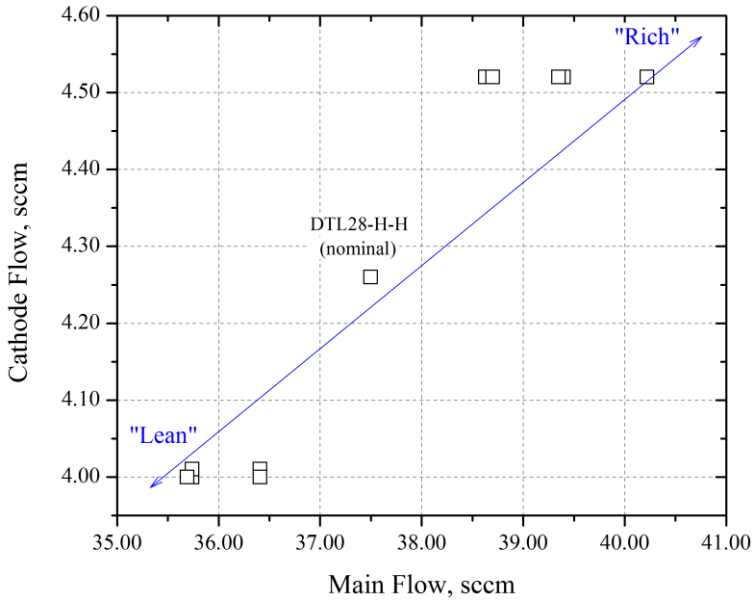

Figure 9. Discharge chamber flow envelope for the system integration test.

B. Algorithm Definition

Verifying the proper execution of the DART flight algorithms was a critical part of the system integration test. Algorithms to operate the NEXT engine have been defined and tested as part of NEXT-C and DART risk reduction tests. The algorithms leverage the work that was completed during the NEXT Phase II development effort, as well as the NSTAR flight projects. The algorithms include sequences to start the engine, regulate the beam current (thrust), and shut off the engine. The algorithms that were characterized for the DART mission are as follows:

1. Cathode Conditioning: Procedure used to prepare thruster cathodes for operation after exposure to contaminating environments.

2. Discharge: Procedure for igniting the neutralizer and then the thruster discharge cathodes.

3. Throttle: Procedure for igniting both hollow cathode assemblies, applying high voltage to the ion optics, and ramping the discharge current to achieve the set-point beam current.

4. Beam Current Regulation: Actively controls the beam current (thrust) during steady-state operation.

5. Shut Down: Procedure for removing input power and propellant flow from an operating thruster.

The Cathode Conditioning and Shutdown procedures from the NEXT-C project replicated those used by NSTAR during flight operations and were also adopted for DART. The Throttle (start-up) and Beam Current Regulation sequences have been described in detail in Refs. [18,19]

V.Test Results

The test results for the thruster, PPU, and SWIL simulator are presented in this section.

A. Thruster Performance

The propellant flow rate was the primary variable of interest with respect to thruster performance. Thruster operation was largely unaffected by changes in the PPU baseplate temperature or the PPU input power bus voltage, which is consistent with prior NEXT integration tests. The performance of the Dev-C thruster was compared to the experimental data obtained during the risk reduction tests, in which the EM4 engine was operated using commercially available power supplies. The Dev-C thruster telemetry were collected from the PPU BoB, and the voltages were corrected to account for the ~40 feet of cable length between the thruster and the digital multi-meter bank. The data below were obtained at the nominal beam voltage (1021 V) and accelerator voltage (-175 V). The discharge voltage and discharge losses (= discharge power required to create 1 A of beam current) as a function of discharge flow rate are shown in Fig. 10. These two parameters were both in-family with EM4 data, with dispersions well within the ranges expected from operating two separate thrusters in two separate facilities[21]

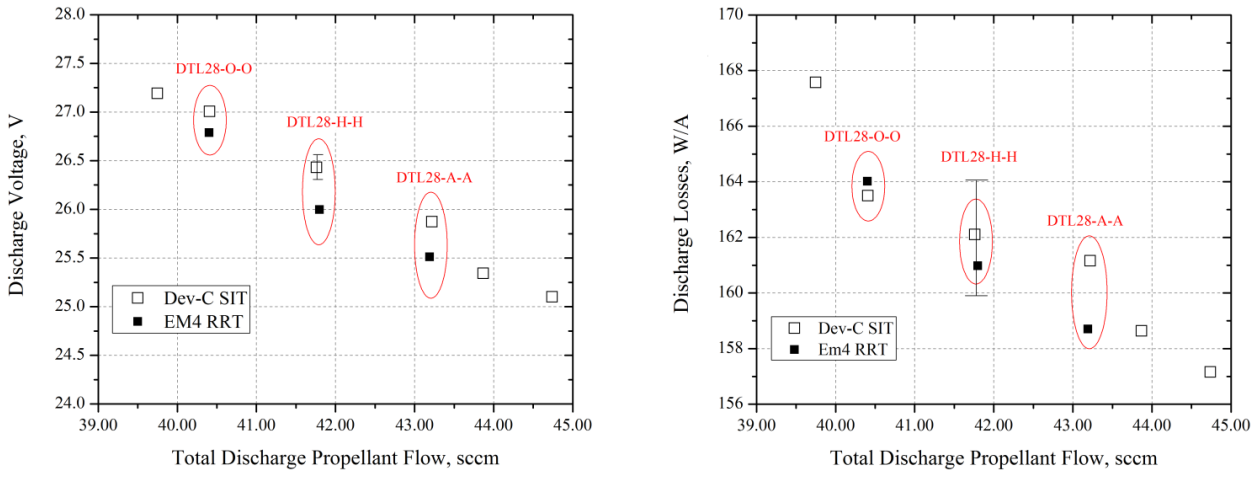

(a) (b)

Figure 10. Discharge voltage and discharge losses as a function of the total propellant flow into the discharge (main + cath).

Figure 11 plots the discharge losses vs the propellant utilization efficiency (lower abscissa) and the discharge flow rate (upper abscissa). The propellant utilization efficiency is defined as the fraction of input propellant mass that is converted into beam ions. The utilization efficiency requires knowledge of the charge state fraction, which was estimated from measurements obtained at The Aerospace Corporation.[17,19] The plot exhibits expected trends, with lower flow rates corresponding to higher discharge losses and higher propellant utilization efficiencies. Operating

the thruster at higher propellant utilization efficiencies results in higher thruster efficiency at the expense of increased erosion of cathode-potential surfaces due to higher discharge voltages and increased production of doubly ionized Xe. Conversely, operating the thruster in a propellant "rich" state results in decreased thruster efficiency, with a slight increase in accelerator grid erosion, due to an increase in charge-exchange ion production. Neither extreme is consequential to thruster service life due to the modest propellant throughput required for DART. The specific impulse and thruster efficiency are shown in Figs. 12 and 13, respectively. The calculated thrust for these conditions is approximately 135 mN, with a specific impulse of 3375 sec and a thruster efficiency of 62% at the nominal condition of DTL28-H-H. Again, the ranges of these two parameters are in-family with baseline EM4 data obtained with a power console, and the thruster performance was deemed to be nominal throughout the test.

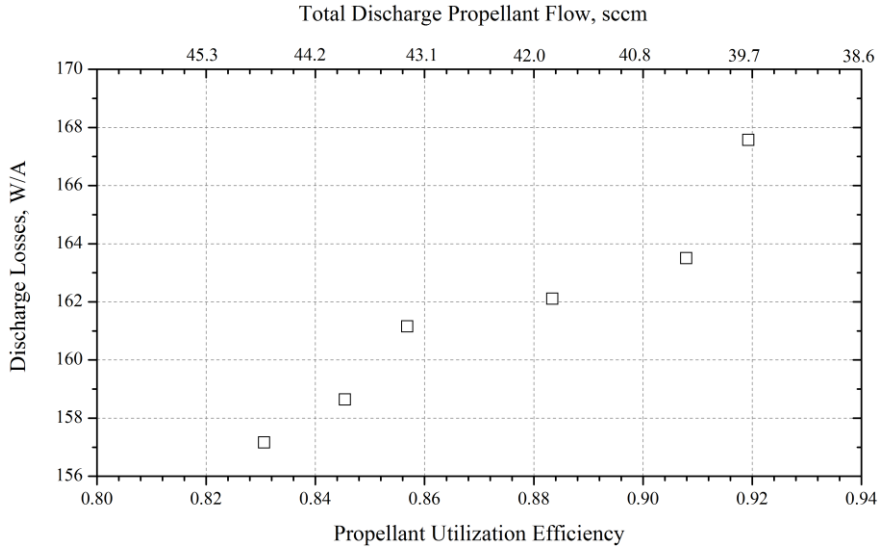

Figure 11. Discharge losses as a function of the propellant utilization efficiency.

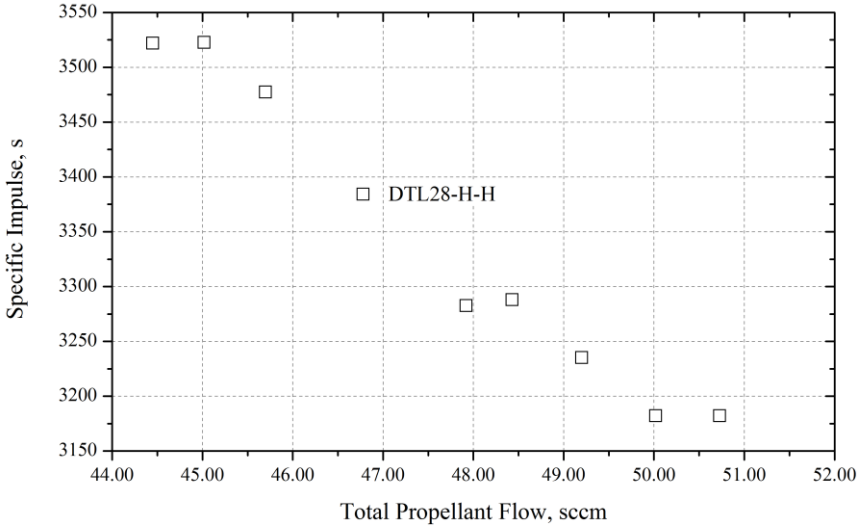

Figure 12. Specific impulse as a function of the total propellant flow (main+cath+neut).

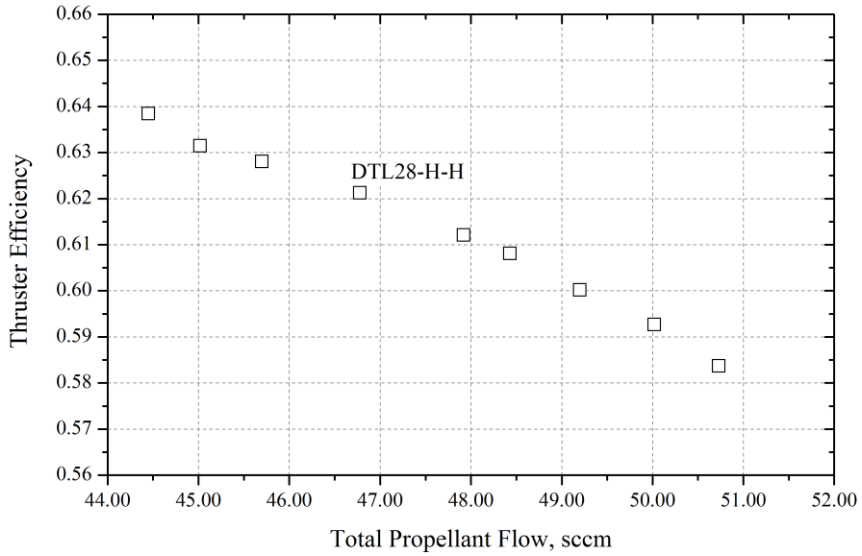

Figure 13. Thruster efficiency as a function of the total propellant flow (main+cath+neut).

1. Thrust Vector Results

The thrust vector (beam current centroid) was continually monitored throughout each test run. During each test-run the thruster was operated in the following manner: 1) cold start to DTL28 using the automated start-up sequence; 2) operate at the DTL28 condition for a specified amount of time with various flow splits; 3) shut off the engine and restart at a different throttle level (beam voltage); 4) operate at this condition for a specified amount of time with several flow splits; 5) shut off the engine at restart at a final throttle level. The data at three different beam voltages are shown in Fig. 14. The thrust vector angel (offset from thruster centerline) typically had an offset of 0.4˚-0.6˚ upon thruster start up, which may be due to the slight radial misalignment of the electrodes. During the cold starts a peak in the thrust vector was observed, which is due to beam steering as the electrode grid gap changes. This peak was absent during the "warm" thruster re-starts. The thrust vector typically reached a steady-state value after approximately 2 hours. There was minimal variation in the thrust vector as the flow splits were changed. This result was expected due to the marginal variations in the discharge power over the conditions tested.

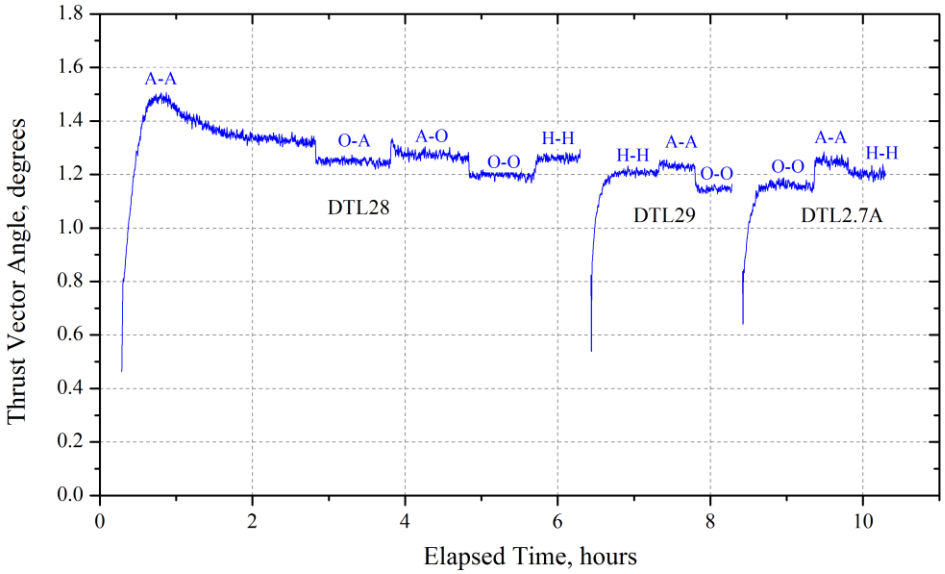

Figure 14. The thrust vector at various beam voltages and flow splits.

2. Algorithm Results

Multiple start-up sequences were demonstrated by transitioning from an off-state to DTL28. The sequences were captured at nominal, high, and low discharge and neutralizer flow rates. The typical 'cold' start-up thruster temperature was approximately 10℃ (as determined from gimbal pad temperatures from prior thruster tests). A baseline start-up script was repeatedly demonstrated, yielding full-thrust operation in less than 8.0 minutes. The sequence incorporates a simultaneous heating of the cathode assemblies, followed by ignition of the neutralizer and discharge cathodes. This approach yields extremely-reliable ignition, and reduces the duration during which the PPU discharge power supply is energized open-circuit. Reliable neutralizer ignition was achieved at lean conditions relative to the NEXT-C specification, with rapid transition post ignition into quiescent spot-mode. No issues (e.g. thruster arcs, electron back-streaming, anomalous thruster telemetry) were encountered during any of the thruster start-ups. Figure 15 shows the discharge voltage V_d, discharge current J_d, beam current J_b, accelerator current J_a and coupling voltage V_g during a start-up sequence. Time (t = 0) corresponds to the initiation of the sequence, that is, when current is applied to the cathode heaters. The discharge voltage and coupling voltage stay within nominal NEXT operating ranges, and reach steady-state values within minutes of high voltage application. The peak ('hump') in accelerator current J_a is likely due to improper steering of the discharge plasma; as the beam current is increased the ions are properly focused through the apertures yielding decreased impingement currents. The peak accelerator current (~ 14 mA) is of short duration and is within the bounds of typical NEXT operation—minimizing any related lifetime concerns. The beam current reaches the set-point value of 2.70 A after 7.5 min, and the beam current regulation regulates the thrust to within 1%. The sequence and thruster response are nearly identical to the baseline EM4 data, verifying the proper execution of the algorithm using the SWIL simulator.

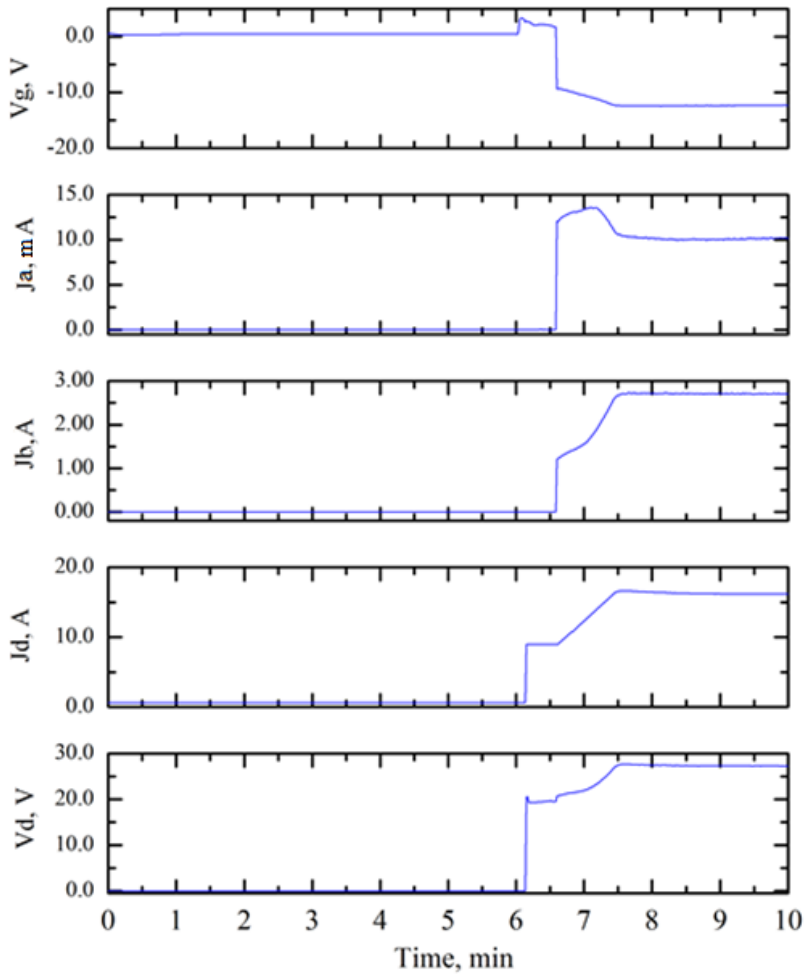

Figure 15. Thruster telemetry during typical start-up sequence.

B. PPU Performance

The PPU's efficiency was the most important PPU performance indicator that was measured in this test. The PPU's efficiency, defined as the sum of the PPU output power from the beam, discharge, accelerator, and neutralizer supplies divided by the total high power bus input power. Note that the PPU's low power bus power was not factored into this calculation, as it constitutes a small percentage of the total power.

The PPU's efficiency was measured as the following parameters were varied:

- PPU Baseplate Temperature (tested at -24℃, 40 ℃, and +55℃)
- PPU Output Power Throttle Level (tested at TL28, TL29, and ETL2.7A)
- PPU Input High Power Bus Voltage (tested at 80V, 100V, and 125V)
- Thruster propellant flow rate (as described in the Thruster section above)

Figure 16 plots the PPU Efficiency at a -24℃ baseplate temperature as output power level, input high power bus, and thruster propellant flow rate were varied.

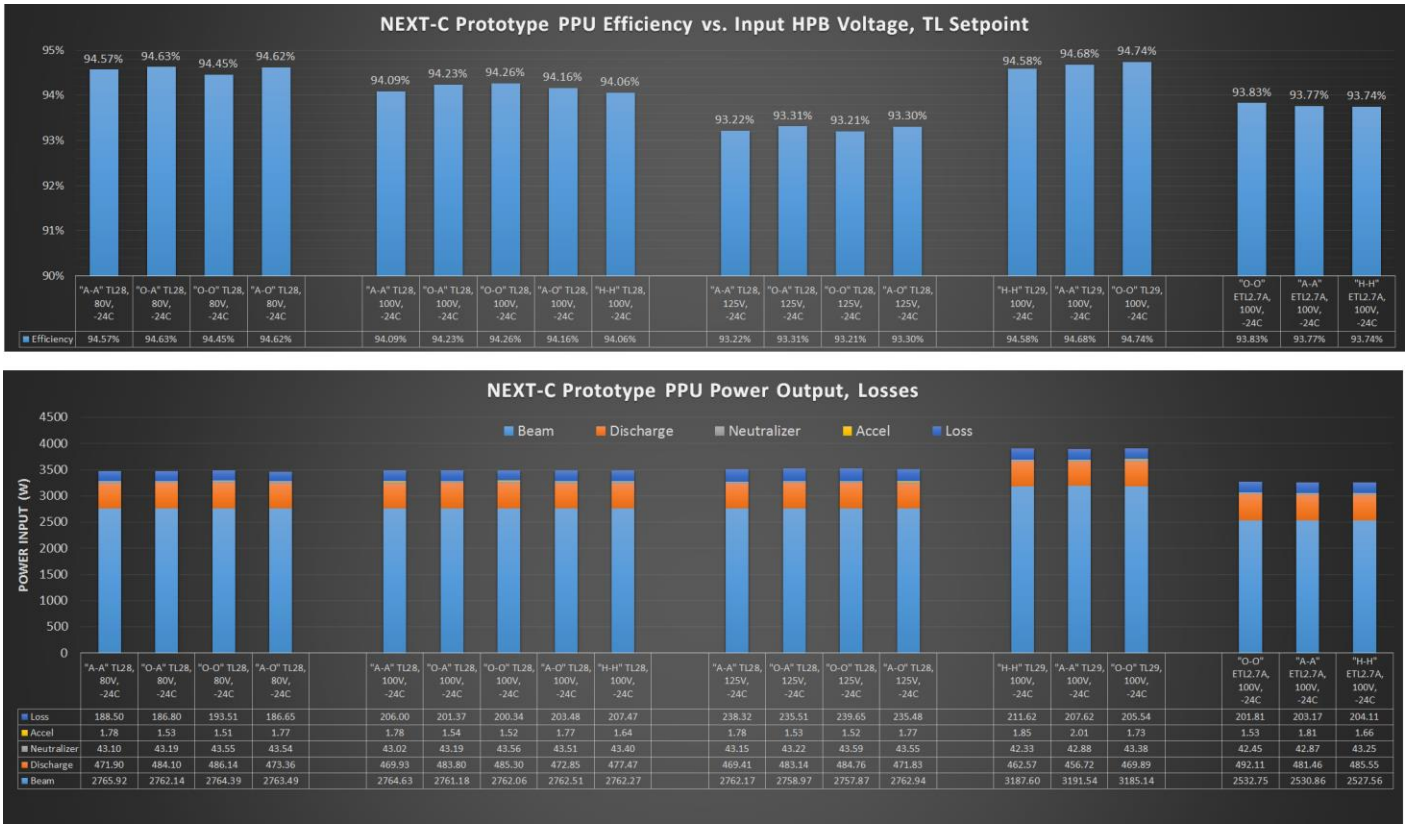

Figure 16. PPU high power bus efficiency, -24℃ baseplate temperature.

Figure 17 plots the PPU Efficiency at a +40℃ baseplate temperature as output power level, input high power bus, and thruster propellant flow rate were varied.

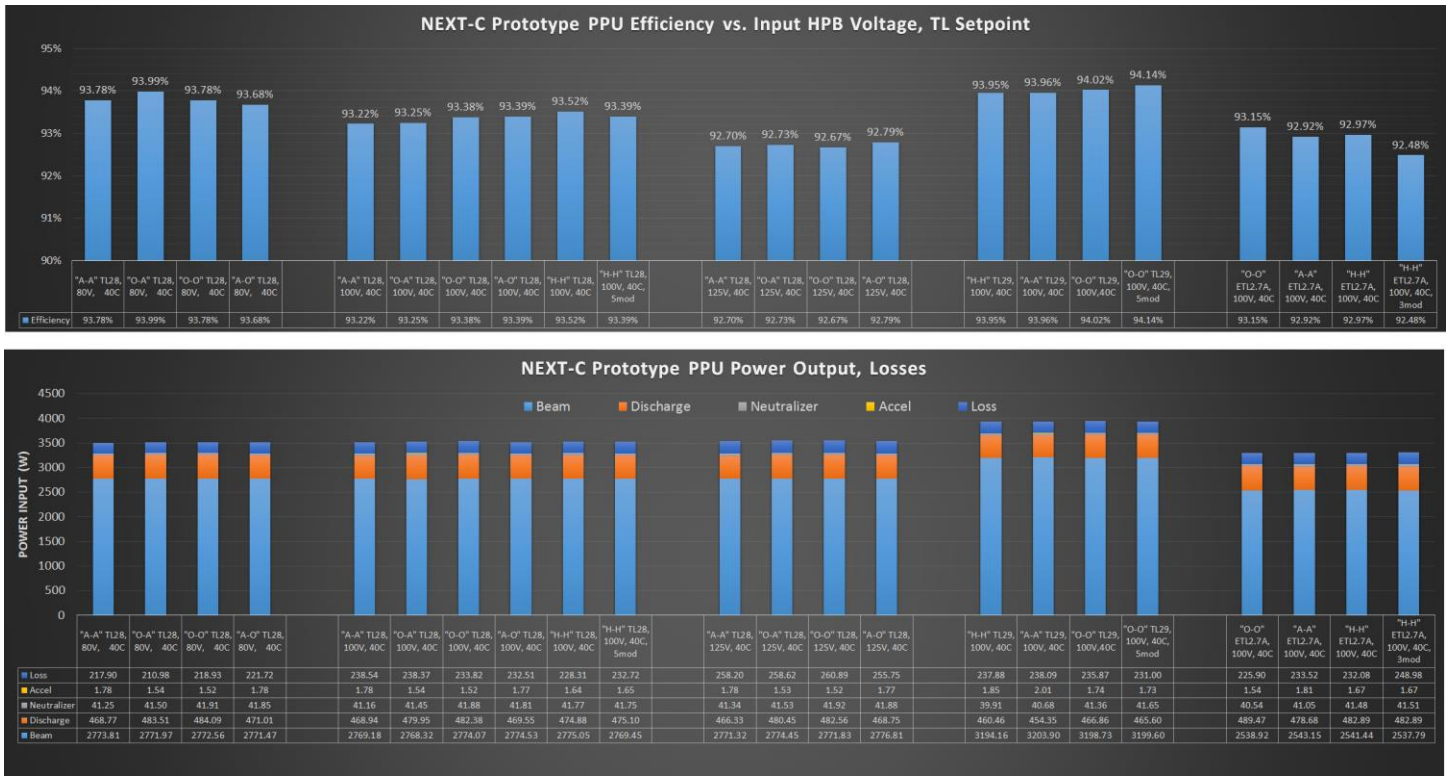

Figure 17. PPU high power bus efficiency, +40℃ baseplate temperature.

Figure 18 plots the PPU Efficiency at a +55℃ baseplate temperature as output power level, input high power bus, and thruster propellant flow rate were varied.

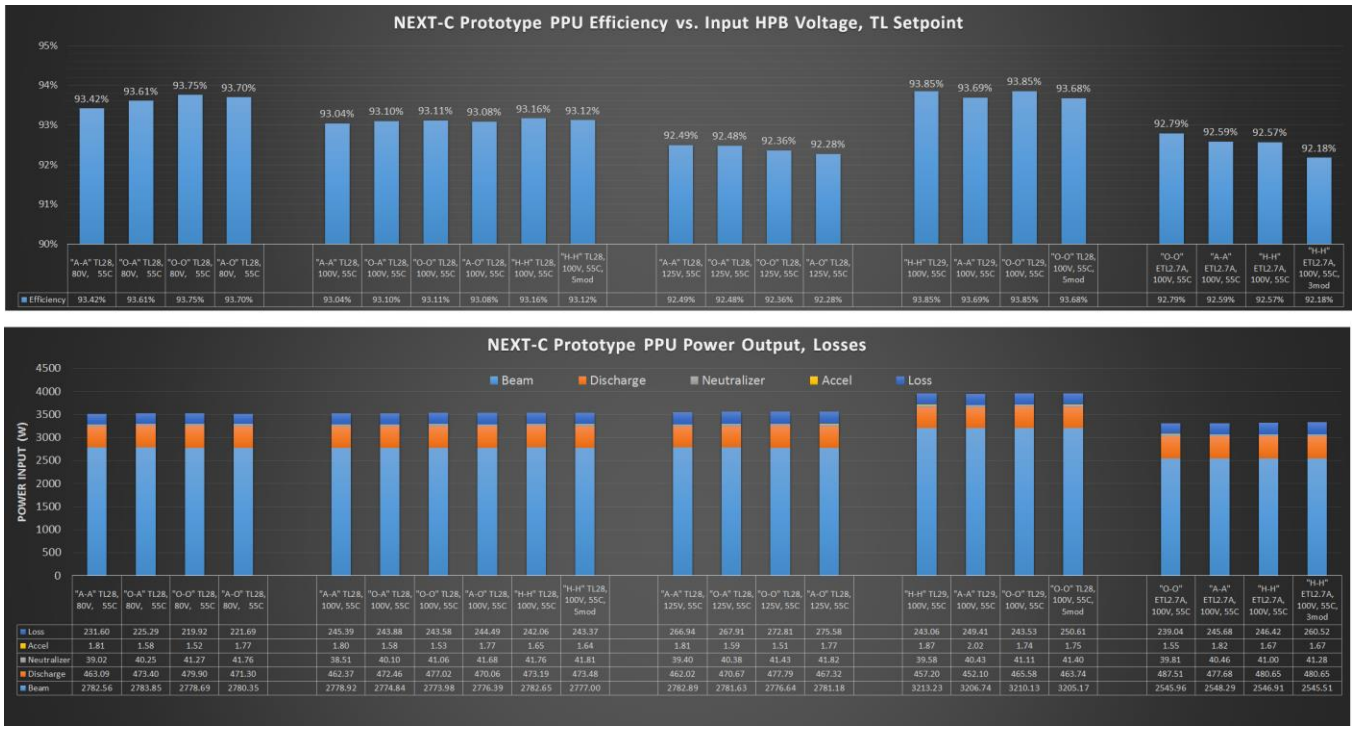

Figure 18. PPU High Power Bus Efficiency, +55℃ Baseplate.

The PPU efficiency data shows many clear trends. The PPU is most efficient at the -24℃ baseplate temperature, and least efficient at +55 C baseplate temperature. The coldest baseplate temperature increases the PPU efficiency by approximately 1% versus the same operation condition at +55℃. The PPU was generally most efficient at 80V input, and least efficient at 125V input.

The PPU efficiency and power input was not significantly impacted by the variations in thruster flow rate. The main impact of the thruster flow rate changes was that lower flowrates caused the discharge and neutralizer supply output voltages to increase as the PPU held their output currents constant. As a result, the larger discharge and neutralizer supply output voltages caused the PPU output power for those supplies to increase slightly, modulating the PPU efficiency.

C. SWIL Performance

The SWIL commands the PPU through each step of cathode conditioning, operating the NEXT-C thruster in diode mode, and firing the NEXT-C thruster with high-voltage beam extraction. Such steps include commanding the PPU to output particular voltages and/or currents at a specific time and verifying specific responses via telemetry. Two examples are included below.

Diode mode is used in early mission operations to warm-up and bake out the thruster by igniting a discharge plasma without beam extraction. As shown in Fig. 19, diode mode begins with pre-heating of the neutralizer and discharge cathodes. The neutralizer cathode is ignited and the SWIL verifies neutralizer cathode keeper current stability. The SWIL then commands discharge ignition and similarly verifies discharge current stability. A specified discharge current is then maintained until a manual shutdown command is sent from the SWIL, as shown in Fig. 19.

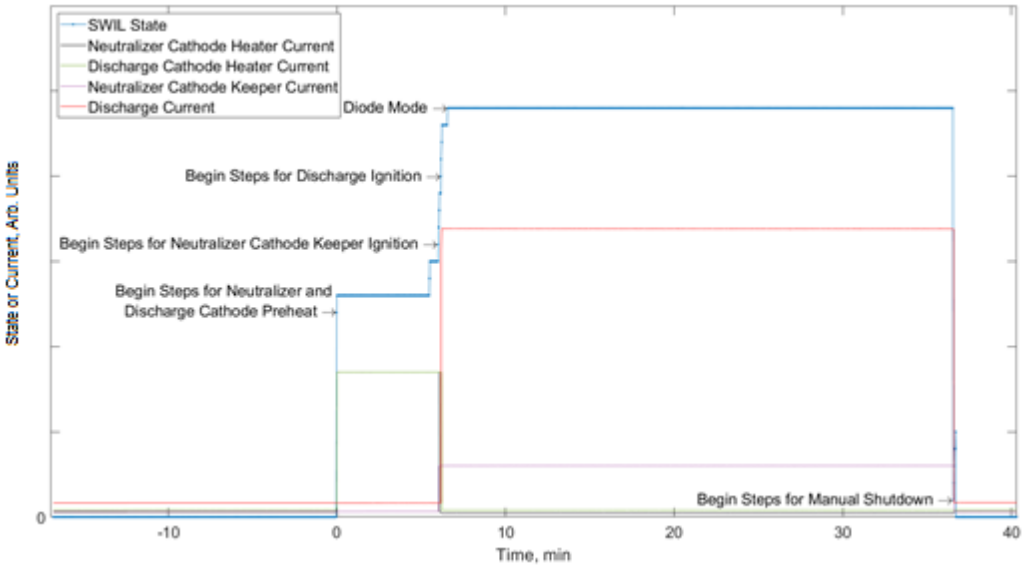

Figure 19. SWIL states and corresponding PPU telemetry for diode mode.

The throttle sequence also begins with pre-heating of the neutralizer and discharge cathodes using their respective cathode heaters. Similar to diode mode, SWIL then commands the PPU to ignite the neutralizer cathode and subsequently verifies neutralizer cathode keeper current stability. The SWIL then proceeds to discharge ignition and discharge current stability check using PPU telemetry. The application of high voltage for ion beam extraction and beam current control are the subsequent steps. Figure 20 shows an example of ignition and subsequent steps to firing at DTL28 in the throttle sequence using the combination of SWIL, engineering model PPU, and Dev-C thruster. Note that neutralizer cathode heater current dropped below nominal amplitude due to long test harness lengths but had no impact on ignition timing.

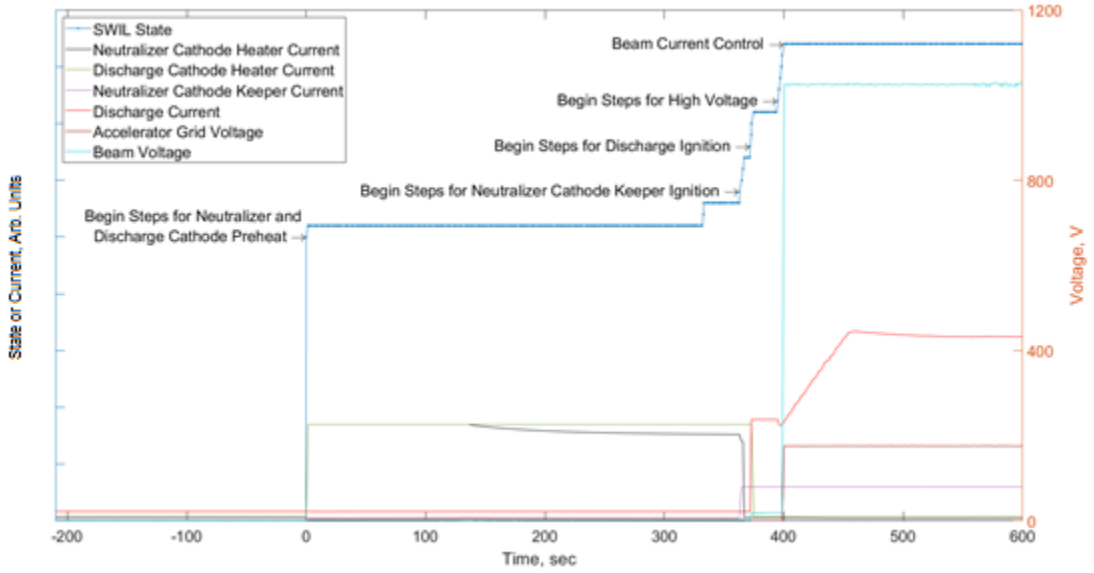

Figure 20. SWIL states and corresponding PPU telemetry for throttle sequence.

The beginning of the throttle sequences resulted in reliable neutralizer cathode and discharge ignitions throughout the system integration test. Figure 21 is a compilation of all startups under the throttle sequence. Ignitions occurred within a relatively narrow time span of approximately 4 seconds for the neutralizer cathode and approximately 6 seconds for the discharge. The SWIL simulator collected telemetry at a rate of approximately 1-2

Hz, so these observed time spans should be considered coarse with a precision on the order of seconds. These ignition times should also be considered representative of the state of the Dev-C thruster at the time of the system integration test and not over the entire lifetime capability of the NEXT-C thruster.

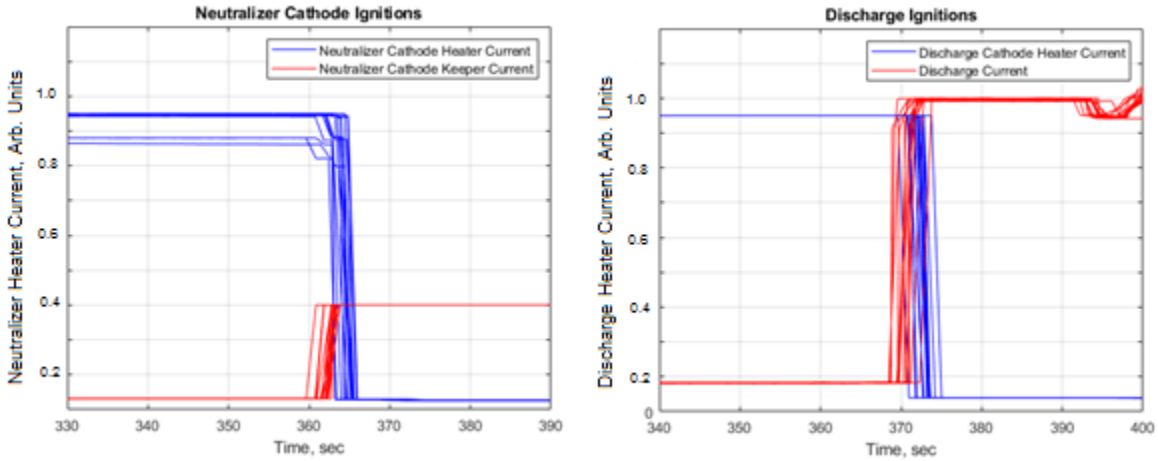

Figure 21. Neutralizer cathode and discharge ignition timings. The neutralizer heater current dropped below its nominal value due to the voltage drops in the transmission lines.

The SWIL and the engineering-model PPU demonstrated stable discharge current control on the Dev-C thruster in order to achieve a steady-state beam current of 2.70 A. Figure 22 shows the compilation of steady-state beam currents from various firing periods during system integration test. Of the firing periods shown, the average beam current measured by SWIL simulator telemetry was 2.71 A for all three DART throttle levels. As shown in the beam current telemetry in Figure 22, the steady-state average beam current tends to be slightly higher than the nominal 2.7 A, though the difference is within the beam current telemetry accuracy. The 3σ variation in the beam current telemetry across all firings at DTL28, DTL29, and DETL2.7A was ±0.02 A or 0.7% of the average beam current. This 3σ magnitude is also approximately equal to the beam current telemetry accuracy. The results demonstrated the efficacy of the SWIL, and were used to further the development of the flight software.

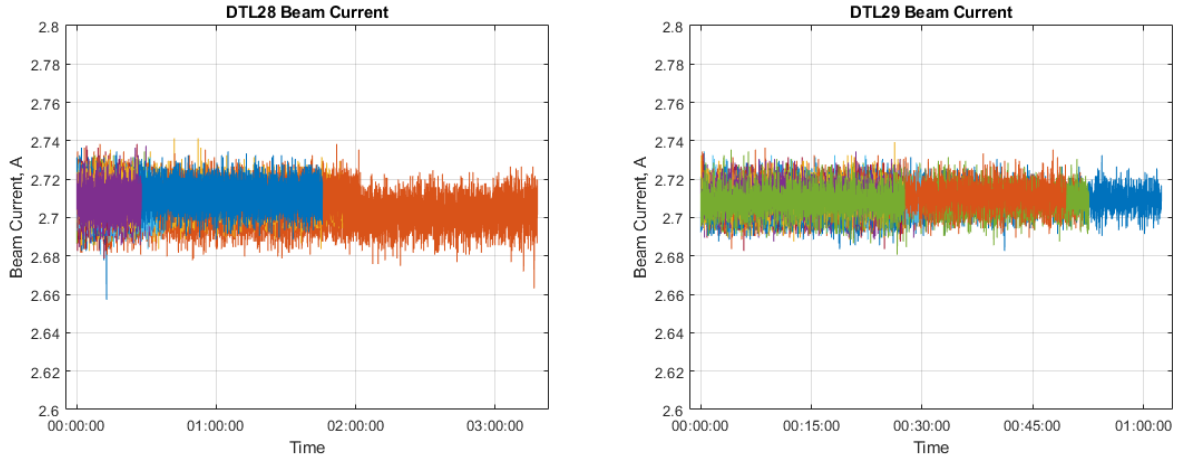

(a) (b)

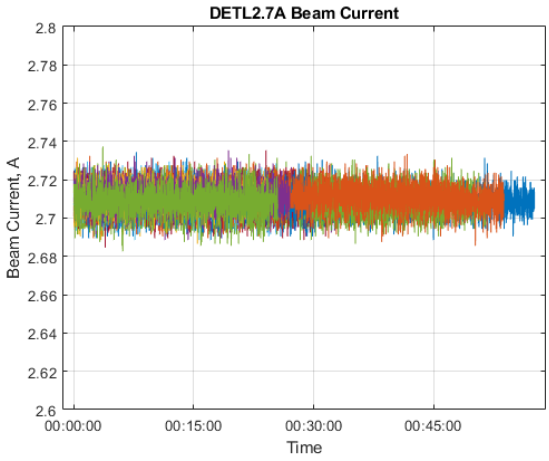

(c)

Figure 22. Steady-state beam currents at the three different throttle levels investigated.

VI. Summary

A single string integration test has been conducted across anticipated DART flight conditions. The system integration test included demonstrations of performance, functionality, and fault handling. The thruster was found to operate nominally across the test matrix, with minimal performance variations as the PPU baseplate temperature or the PPU input power bus voltage were varied. The performance of the engine compared favorably to baseline risk reduction data that was obtained with a power console and the EM4 engine. The thrust vector (beam current centroid) was monitored throughout each test run, and was found to be largely invariant with changes in propellant flow. Multiple start-up sequences were demonstrated by transitioning from an off-state to DART conditions. The SWIL flawlessly executed the DART flight algorithms across different input conditions. In all cases the beam current was controlled to within 0.7%, approximately equal to the beam current telemetry accuracy. The PPU efficiency was characterized over a range of test conditions. The PPU efficiency data shows increased performance at colder temperatures and lower input voltages. The test successfully demonstrated the functionality of the integrated system at DART conditions, and the results of the test were used, as applicable, in the build of flight software and hardware.

Appendix: Thruster Conditions Tested During the System Integration Test

Throttle Level	Beam Current, A	Beam Voltage, V	Accel. Voltage, V	Main Flow, sccm	Cath. Flow, sccm	Neut. Flow, sccm
DETL2.7-AAA-AA	2.700	936	-175	40.179	4.517	6.000
DETL2.7-AAA-A	2.700	936	-175	40.179	4.517	5.300
DETL2.7-AA -A	2.700	936	-175	39.428	4.517	5.300
DETL2.7-A-A	2.700	936	-175	38.682	4.517	5.300
DETL2.7-H-H	2.700	936	-175	37.550	4.262	5.000
DETL2.7-AAA-O	2.700	936	-175	40.179	4.517	4.700
DETL2.7-O-O	2.700	936	-175	36.428	4.006	4.700
DETL2.7-P-O	2.700	936	-175	35.762	4.006	4.700
DETL2.7-P-AA	2.700	936	-175	35.762	4.006	6.000
DTL28-AAA-AA	2.700	1021	-175	40.179	4.517	6.000
DTL28-AAA-A	2.700	1021	-175	40.179	4.517	5.300
DTL28-AA-A	2.700	1021	-175	39.428	4.517	5.300
DTL28-A-A	2.700	1021	-175	38.682	4.517	5.300
DTL28-O-A	2.700	1021	-175	36.428	4.006	5.300
DTL28-P-A	2.700	1021	-175	35.762	4.006	5.300
DTL28-H-H	2.700	1021	-175	37.550	4.262	5.000
DTL28-A-O	2.700	1021	-175	38.682	4.517	4.700
DTL28-AA-O	2.700	1021	-175	39.428	4.517	4.700
DTL28-AAA-O	2.700	1021	-175	40.179	4.517	4.700
DTL28-O-O	2.700	1021	-175	36.428	4.006	4.700
DTL28-P-O	2.700	1021	-175	35.762	4.006	4.700
DTL28-P-AA	2.700	1021	-175	35.762	4.006	6.000
DTL29-A-A	2.700	1179	-200	38.682	4.517	5.300
DTL29-AA-A	2.700	1179	-200	39.428	4.517	5.300
DTL29-H-H	2.700	1179	-200	37.550	4.262	5.000
DTL29-O-O	2.700	1179	-200	36.428	4.006	4.700
DTL29-P-O	2.700	1179	-200	35.762	4.006	4.700

Acknowledgments

The authors thank Kevin McCormick, Mike Pastel, and Rich Polak for their support with test preparations and set-up. This DART mission is funded through NASA's Planetary Defense Program Office and NEXT-C has been developed through NASA's Science Mission Directorate.

.

References

[1]Patterson, M., Foster, J., Haag, T., Rawlin V., Soulas, G., Roman, R., "NEXT: NASA's Evolutionary Xenon Thruster," *38th AIAA/ASME/SAE/ASEE Joint Propulsion Conference & Exhibit,* Indianapolis, IN, AIAA-2002-3832.

[2]Oleson, S., Gefert, L., Sims, J., Noca, M., Patterson, M., and Benson, S., "Mission Advantages of NEXT: NASA's Evolutionary Xenon Thruster," *38th AIAA/ASME/SAE/ASEE Joint Propulsion Conference & Exhibit*, Indianapolis, IN, AIAA-2002-3969.

[3]Soulas, G., Patterson, M., Pinero, L., Herman, D., and Snyder, J., "NEXT Single String Integration Test Results," *45th AIAA/ASME/SAE/ASEE Joint Propulsion Conference & Exhibit*, Denver, CO, AIAA-2009-4816.

[4]Patterson, M., Foster, J., McEwen, H., Herman, D., Pencil, E., and VanNoord, J., "NEXT Multi-Thruster Array Test - Engineering Demonstration," *42nd AIAA/ASME/SAE/ASEE Joint Propulsion Conference & Exhibit*, Sacramento, CA, AIAA-2006-5180.

[5]Snyder, J.S., Anderson, J.R., VanNoord, J.L., and Soulas, G.C., "Environmental Testing of the NEXT PM1R Ion Engine," *30th International Electric Propulsion Conference*, Florence, Italy, IEPC-2007-276.

[6]Soulas, G., Domonkos, M., and Patterson, M., "Wear Test Results for the NEXT Ion Engine," *39th AIAA/ASME/SAE/ASEE Joint Propulsion Conference and Exhibit*," Huntsville, AL, AIAA-2003-4863.

[7]Shastry, R., Herman, D.A., Soulas, G.C., and Patterson, M.J., "End-of-test Performance and Wear Characterization of NASA's Evolutionary Xenon Thruster (NEXT) Long-Duration Test," *50th AIAA/ASME/SAE/ASEE Joint Propulsion Conferenc*e, Cleveland, OH, AIAA-2014-3617.

[8]Fisher, J., et al., "NEXT-C Flight Ion Propulsion Development Status," *35th International Electric Propulsion Conference*, Atlanta, GA, IEPC-2017-218.

[9]Shastry, R., Soulas, G., Aulisio, M., and Schmidt, G., "Current Status of NASA's NEXT-C Ion Propulsion System Development Project," *68th International Astronautical Congress*, Adelaide, Australia, IAC-17.C4.4.3.

[10]Hoskins, A., Wilson, F., Patterson, M., Soulas, G., Polaha, J., Talerico, L., "Development of a Prototype Model Ion Thruster for the NEXT System," *40th AIAA/ASME/SAE/ASEE Joint Propulsion Conference and Exhibit*, Fort Lauderdale, FL, AIAA-2004-4111.

[11]Soulas, G., Domonkos, M., and Patterson, M., "Performance Evaluation of the Next Ion Engine," 39*th AIAA/ASME/SAE/ASEE Joint Propulsion Conference and Exhibit*, Hunstville, AL, AIAA-2003-5278.

[12]Herman, D., Soulas, G., Patterson, M., "Performance Evaluation of the Prototype-Model NEXT Ion Thruster," *43rd AIAA/ASME/SAE/ASEE Joint Propulsion Conference & Exhibit*, Cincinnati, OH, AIAA-2007-5212.

[13]Diamant, K., Pollard, J., Crofton, M., Patterson, M., and Soulas, G., "Thrust Stand Characterization of the NASA NEXT Thruster," *46th AIAA/ASME/SAE/ASEE Joint Propulsion Conference & Exhibit*, Nashville, TN, AIAA-2010-6701.

[14]Pinero, L.R., and Benson, S.W.., "NEXT Engineering Model PPU Development, Progress and Plans," *47th AIAA/ASME/SAE/ASEE Joint Propulsion Conference & Exhibit*, San Diego, CA, AIAA-2011-5659.

[15]Aulisio, M.V., et al., "Status of the Development of Flight Power Processing Units for the NASA's Evolutionary Xenon Thruster – Commercial (NEXT-C) Project," 52*th AIAA/ASME/SAE/ASEE Joint Propulsion Conference & Exhibit*, Salt Lake City, UT, AIAA-2016-4519.

[16]C. Heistand et al., "DevOps for Spacecraft Flight Software," 2019 IEEE Aerospace Conference, Big Sky, MT, USA, 2019, pp. 1-16.

[17]Thomas, R.E., Patterson, M.J., Crofton, M.W., John, J.W., "NEXT Ion Propulsion System Risk Mitigation Tests in Support of the Double Asteroid Redirection Test Mission," 55*th AIAA/ASME/SAE/ASEE Joint Propulsion Conference & Exhibit*, Indianapolis, IN..

[18]Thomas, R.E., Patterson, M.J., Soulas, G.C., "Development and Validation of Autonomous Operational Sequences for the NEXT Ion Propulsion System," 52*th AIAA/ASME/SAE/ASEE Joint Propulsion Conference & Exhibit*, Salt Lake City, UT, AIAA-2016-5077.

[19]Thomas, R.E., Patterson, M.J., and Soulas, G.C., "Algorithm Validation Testing of the NEXT Ion Propulsion System," *63rd Joint Army-Navy-NASA-Air Force Propulsion Meeting*, Newport News, VA, 2016.

[20]Young, J.A., Matlock, T., Nakles, M., Crofton, M.W., Patterson, M.J., Arthur, N.A., and John, J., "Far Field Plume Distribution and Divergence for NEXT: DART Mission," *AIAA Scitech 2019 Forum*, Orlando, FL, AIAA-2019-1243.

[21]Soulas, G. and, Patterson, M., "NEXT Ion Thruster Performance Dispersion Analyses," 43rd *AIAA/ASME/SAE/ASEE Joint Propulsion Conference & Exhibit*, Cincinnati, OH, AIAA-2007-5213.